Click Here for Full Article

Use of vegetation properties from EOS observations for land-climate modeling in East Africa

Jianjun Ge,[1] Jiaguo Qi,[2,3] and Brent Lofgren[4]

[1] Land use/cover change has been recognized as a key component in global climate change. Information on land surface biophysical properties and climatic variables based on in situ data fail to resolve the fine-scale variability that exists in many parts of the world, including East Africa. In this study, we used the NASA's Earth Observing System (EOS) products to improve the representation of the land surface in a regional climate model as well as assess the model performance. The Moderate Resolution Imaging Spectroradiometer (MODIS) data of leaf area index (LAI) and vegetation fractional cover (VFC) were directly incorporated in the Regional Atmospheric Modeling System (RAMS). The model was validated in terms of the land surface temperature (LST), utilizing the MODIS LST data from both Terra and Aqua satellites. Compared with the built-in land surface, the ingested MODIS LAI and VFC greatly improved the spatial and temporal dynamics of vegetation in East Africa. Three experiments were carried out for the year of 2003 to test the impacts of land surface conditions. The results showed that the spatial, seasonal, and diurnal characteristics of the RAMS simulated LST were improved because of MODIS LAI and VFC. Specifically, the Intertropical Convergence Zone (ITCZ)–related migration, bimodal temporal variation, and monthly averaged diurnal cycles of LST were more realistically reproduced. The need to realistically represent the spatial and temporal distribution of vegetation is thus highlighted, and the value of the EOS observations for the land-climate modeling is demonstrated.

1. Introduction

[2] Land is the lower boundary of the atmosphere and thus a major component of the climate system. Human modification of the land surface impacts regional to global climate processes by changing the fluxes of mass and energy between ecosystems and the atmosphere [*Chase et al.*, 1999; *Houghton et al.*, 1999; *Pielke et al.*, 2002]. Over the past decades, land use/cover has been widely recognized as a critical factor mediating socioeconomic, political and cultural behavior and global climate change [*International Geosphere-Biosphere Programme*, 1990; *Intergovernmental Panel on Climate Change*, 2000]. Interactions between the biosphere and atmosphere have therefore been the focus of numerous climate modeling studies [e.g., *Xue*, 1997; *Pielke et al.*, 1999; *Chase et al.*, 2000; *Lu et al.*, 2001; *DeFries et al.*, 2002; *Taylor et al.*, 2002; *Feddema et al.*, 2005; *Ge et al.*, 2007].

[3] In order to simulate the impacts of anthropogenic land surface changes, climate models require parameterizations of the land surface, which generally consist of two elements: mathematical algorithms for the description of the processes involved and numerical parameter values required to do calculations [*Dickinson*, 1995]. Ever since *Deardorff*'s [1978] pioneering work, land surface models have evolved from quite simple treatments of the surface energy, moisture and momentum exchanges to increasingly complex descriptions [*Dickinson et al.*, 1991; *Sellers et al.*, 1997; *Pitman*, 2003]. Because of lack of observations, biophysical surface variables in land surface models (e.g., leaf area index (LAI), vegetation fractional cover (VFC), and albedo) were initially not based on any particular observation data but were guided by past literature or intelligent guesses [*Dickinson et al.*, 1986]. Biophysical values were usually assigned to broad vegetation classes by means of a lookup table, and seasonal variations of vegetation were represented by simple mathematical equations. This simple treatment of surface biophysical properties severely limited the detailed modeling of land-climate interactions.

[4] Remote sensing from satellites has begun to serve an essential role as the means of obtaining global data to improve the land surface representation in climate models. Various attempts have been made to use remotely sensed biophysical variables in climate modeling studies. For example, the Advanced Very High Resolution Radiometer

[1]Department of Geography, Oklahoma State University, Stillwater, Oklahoma, USA.
[2]Department of Geography, and Center for Global Change and Earth Observations, Michigan State University, East Lansing, Michigan, USA.
[3]Also at Institute of Geographic Sciences and Natural Resources Research, Chinese Academy of Sciences, Beijing, China.
[4]Great Lakes Environmental Research Laboratory, NOAA, Ann Arbor, Michigan, USA.

(AVHRR) based normalized difference vegetation index (NDVI) was used to determine the temporal variation of LAI and fraction of absorbed photosynthetically active radiation (fPAR) in the revised Simple Biosphere Model (SiB2) [*Sellers et al.*, 1996a, 1996b]. LAI derived from AVHRR NDVI was directly incorporated into the Regional Atmospheric Modeling System (RAMS) to investigate the sensitivity of regional climate simulations to changes in vegetation [*Lu and Shuttleworth*, 2002], and it was found that regional climates were sensitive to the land surface heterogeneity and seasonal changes in vegetation phenology. A set of biophysical parameters, created from the Moderate Resolution Imaging Spectroradiometer (MODIS), were tested in a global model to investigate the impacts of improved land surface representations [*Zhou et al.*, 2003; *Tian et al.*, 2004], and the results showed that biases in surface air temperature decreased and simulated surface physical evaporation and transpiration were closer to reality. These studies indicated the importance of realistic representation of both the spatial and temporal distribution of vegetation in climate modeling.

[5] Furthermore, remotely sensed biophysical variables have been used in many numerical weather prediction studies, such as *Crawford et al.* [2001], *Santanello and Carlson* [2001], *Kurkowski et al.* [2003], *Yucel* [2006], and *de Foy et al.* [2006]. These studies found that making use of remote sensing surface data leads to improved meteorological simulations such as heat wave forecasting, daytime temperature prediction, and modeling wind circulation patterns and urban heat island. The difference between numerical weather prediction and climate simulations is that numerical weather prediction depends crucially on the initial state of the atmosphere. On the other hand, climate simulations are run for sufficiently long periods of time (typically more than one month) that they are insensitive to the initial conditions but dependent on boundary conditions such as ocean temperature, land use, and greenhouse gas concentrations [*Giorgi and Mearns*, 1999]. This study includes some parts of the climate system such as a full treatment of atmospheric dynamics, thermodynamics and moisture processes, along with a soil-vegetation-atmosphere transfer (SVAT) scheme. However, unlike some other climate models it does not include a fully integrated ocean, but treats ocean surface temperature as a prescribed boundary condition.

[6] The performance of climate models needs to be evaluated by comparing observed and modeled variables such as precipitation and air temperature. The major problem with traditional meteorological observations when used to validate models is their poor representation of the grid point average simulated by a model. More importantly, well documented station observations of climate variables are mainly located in populated and industrialized parts of the world [*Williams et al.*, 2000]. For the East Africa region in this study (Figure 1), weather station data are extremely scarce [*Ge*, 2007]. Spatially, there are very few stations in Congo, Tanzania and east Kenya. Temporally, few existing stations have continuous time series of observations with consistent quality. This brings formidable challenges for validation of land-climate modeling studies in this region.

[7] The overarching goal of NASA's Earth Observing System (EOS) program is to provide global measurements over long time periods to improve computer models that can accurately predict the causes and effects of climate change [*Justice et al.*, 2002]. MODIS is the primary EOS instrument for global monitoring of terrestrial ecosystems. It provides high radiometric sensitivity in 36 spectral bands with spatial resolutions ranging from 250 m to 1 km. Two EOS satellites, Terra and Aqua, have been successfully launched into sun-synchronous orbits in December 1999 and May 2002 respectively, both carrying the MODIS sensor. The Terra overpass time is around 1030 local solar time in its descending mode and 2230 local solar time in ascending mode. The Aqua overpass time is around 1330 local solar time in ascending mode and 0130 local solar time in descending mode. MODIS, flying on these two satellites, therefore can obtain valuable diurnal variation information which is more suitable for regional and global climate change studies. A new generation of land surface products has been produced from the MODIS data such as LAI, albedo, the Enhanced Vegetation Index (EVI), the Land Surface Temperature (LST), etc. [*Justice et al.*, 2002; *Wang et al.*, 2004; *Huete et al.*, 2002; *Wan et al.*, 2004]. The enhanced spectral, spatial, radiometric, and geometric quality of MODIS data provides a greatly improved basis for monitoring and mapping the global land surface relative to AVHRR data [*Friedl et al.*, 2002; *Justice et al.*, 2002].

[8] The objectives of this paper are to use EOS MODIS products to improve the land surface representation in a regional climate model and evaluate the model outputs. Monthly LAI and VFC images are directly incorporated in the regional model. Land surface processes and some biophysical parameters (e.g., albedo and transmissivity) strongly depend on the value of LAI and VFC in the model used in this study. The assumption is that MODIS land surface products provide a more realistic vegetation distribution and, therefore, can potentially improve the regional climate simulations. The impacts of improved land surface are examined by comparing seasonal and diurnal MODIS LST with model simulated LST. This is the first such effort to fully utilize the LST observations from both EOS Terra and Aqua satellites for evaluating regional climate models. In addition, precipitation data from other satellite observations are used for the validation. The advantage of using EOS observations in land-climate modeling is demonstrated. A detailed description of model and data is given in section 2. The results and discussion are presented in sections 3 and 4, and the major conclusions are reviewed in the final section.

2. Methods and Data

[9] The regional climate model used for the numerical simulations in this work was the Regional Atmospheric Modeling System (RAMS) Version 4.4 [*Pielke et al.*, 1992; *Cotton et al.*, 2003]. Here, "regional climate model" means a limited area model with high resolution, generally with grid spacing less than 100 km, run for a simulation time of more than approximately one month length, so that the initial atmospheric conditions have been forgotten [*Jacob and Podzun*, 1997]. Figure 1 shows the study area in East Africa illustrated by a new land cover data set, the Global Land Cover (GLC) 2000 for Africa [*Mayaux et al.*, 2004]. This data set was developed by the Joint Research Centre's Global Vegetation Unit based primarily on SPOT VEGETATION daily 1 km data, which were acquired from
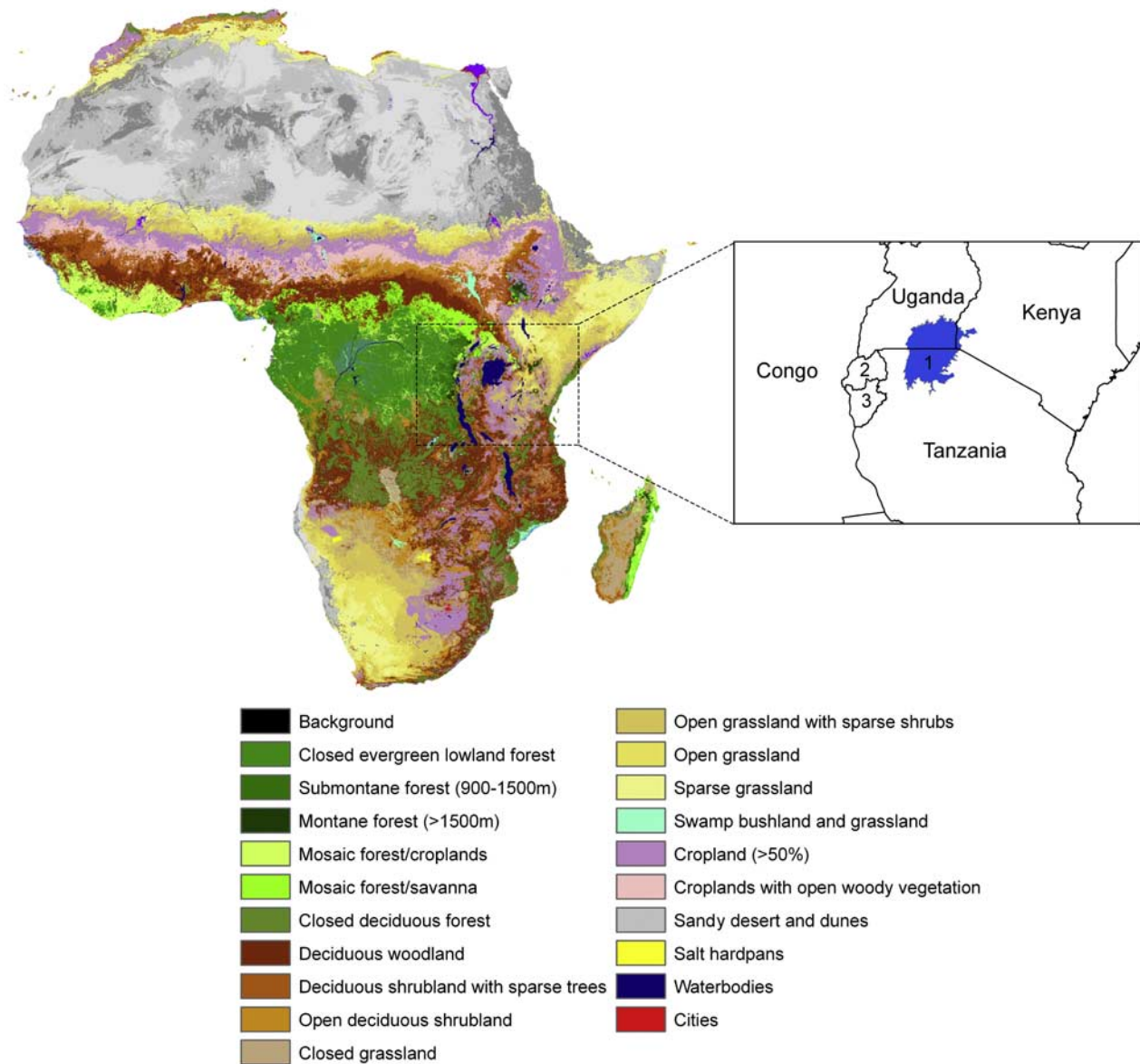
Figure 1. Study area illustrated by GLC2000 for Africa. Areas 1, 2, and 3 refer to Lake Victoria, Rwanda, and Burundi, respectively.

1 November 1999 to 31 December 2000. The GLC2000 for Africa was downloaded at http://www-gem.jrc.it/glc2000/. The study area includes Kenya, Uganda, Tanzania, Congo, Rwanda, Burundi and a small section of Indian Ocean. The largest inland water body is Lake Victoria (Figure 1). RAMS has been found to perform well in various mesoscale modelings in East Africa [e.g., *Mukabana and Pielke*, 1996]. In this study, three numerical experiments were carried out to evaluate the impacts of the improved land surface parameterization in RAMS. In the first experimental run, here called the "default" (DEF) run, the default land surface representation in RAMS was used, which includes the Olson Global Ecosystem (OGE) land cover data set with built-in biophysical values. In the second run, here called the "GLC" run, the built-in LAI and VFC were used but with OGE land cover replaced by GLC2000 to test the effect of this new land cover data set. Both GLC2000 and

MODIS derived LAI and VFC were used for the third run, which is called "GLC + LAI + VFC" in this study. The year 2003 was chosen for all three experiments. Precipitation in 2003 was close to the long-term average (http://cics.umd.edu/~yin/GPCP/main.html>) and all MODIS products are available in 2003.

2.1. RAMS and Configuration

[10] RAMS is a three-dimensional, nonhydrostatic, general purpose atmospheric simulation modeling system, which solves equations of motion, heat, moisture, and mass continuity in a terrain-following coordinate system. It is capable of both numerical weather prediction and regional climate simulation.

[11] The SVAT scheme employed in RAMS is the Land Ecosystem-Atmosphere Feedback model, version 2 (LEAF-2) [*Lee*, 1992; *Walko et al.*, 2000]. LEAF-2 represents the storage
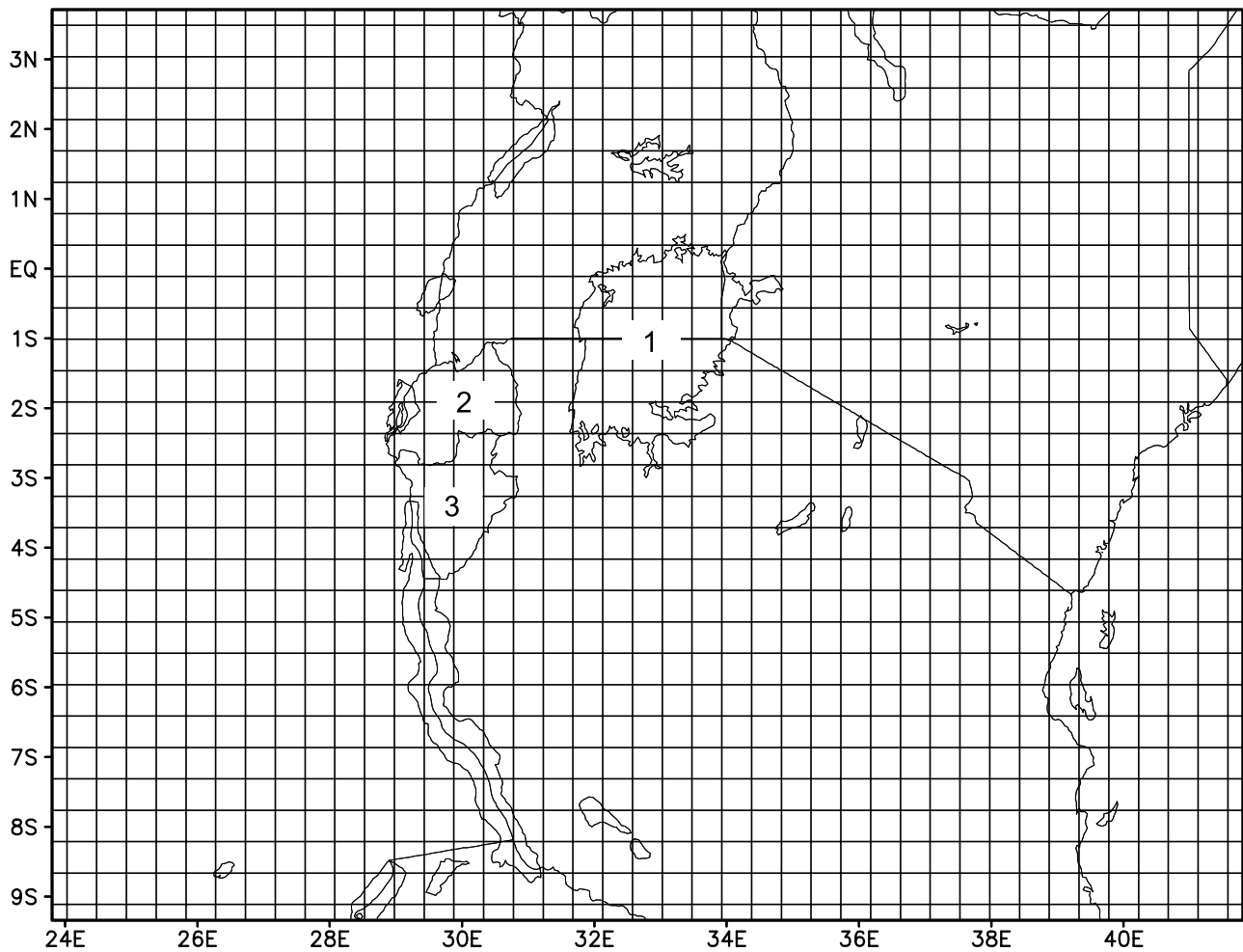
Figure 2. RAMS domain with Δx = 50 km. Areas 1, 2, and 3 refer to Lake Victoria, Rwanda, and Burundi, respectively.

and vertical exchange of water and energy in multiple soil layers, temporary surface water or snow cover, vegetation and canopy air. The LEAF-2 is able to represent fine-scale surface variations by dividing surface grid cells into subgrid patches. Each patch has its own land cover type and soil texture class, and it responds to and influences the overlying atmosphere in its own unique way according to its fractional area of coverage. The biophysical characteristics, such as LAI, VFC, albedo, etc., are then defined in a lookup table for the land cover type each patch possesses (see http://www.atmet.com/html/docs/rams/RT1-leaf2-3.pdf for the built-in lookup table for biophysical characteristics defined in LEAF-2). Of these biophysical variables, LAI and VFC are assumed to have a simple seasonal dependence, which is the function of a cosine distribution, latitude and time of year. Vegetation is assumed to peak in late July (Julian day = 200) in the northern hemisphere and the reverse in the southern hemisphere. For locations close to the equator, such as a large part of East Africa in this study, LEAF-2 assumes that seasonal variation is reduced to zero. As a result, the built-in spatial and temporal vegetation variations are extremely unrealistic for near-equatorial regions. In the experiments presented here, the number of patches per grid cell was set to ten for a relatively detailed representation of

the land surface. One patch is allocated for water in all grid cells.

[12] A single grid with 50 km horizontal grid spacing was used as the model domain (Figure 2). When RAMS is run for a short term (days or a couple of weeks), a multiple nesting paradigm is typically followed in which the coarsest grid has the approximate horizontal scale as the reanalysis data. *Castro et al.* [2005] found that a coarse outer grid may introduce undesirable weakening of large-scale atmospheric variability for long-term (more than 2 weeks) model integrations, and they suggested a single grid paradigm which directly assimilates the reanalysis to the mesoscale grid. Bypassing the coarser grid may also avoid the problem of using different parameterization schemes on different grids which may introduce additional uncertainties. For the land surface, the standard RAMS 30-arc sec topography data set was used. The grid extended over 32 vertical levels, with a layer thickness of 80 m near the surface and stretching to 1900 m at the top of the domain. The model was driven by 6-hourly lateral boundary conditions derived from the National Centers for Environmental Prediction (NCEP) atmospheric reanalysis product [*Kalnay et al.*, 1996]. The model time step was 90 s with the output period set to every 3 h. At each time step, the reanalysis data were nudged over five outer grid points. No interior nudging was applied as it

may mitigate the strength of surface boundary forcings [*Ge et al.*, 2007].

[13] The soil model in LEAF-2 consisted of 11 vertical layers spanning a depth of 2.1 m. The topsoil layer was 3 cm in depth, with lower levels becoming progressively thicker. The initial soil temperature was set with an offset of the lowest level atmospheric temperature. For example, the deepest soil level initially had a temperature 5 K warmer than the initial temperature of the lowest atmospheric level. The moisture content of the soil was initialized as 35% of the saturation value, uniformly over the domain. RAMS was spun up over six months starting from July, the beginning of the dry season, to December 2002, and this time period was omitted in the analysis. Soil moisture can play an important role in surface atmosphere interactions particularly through moisture "memory." The presence of soil moisture influences the partitioning of latent and sensible heat, thereby affecting the development of shallow convection. However, soil types in East Africa are poorly mapped, and available soil moisture values for the region are speculative because of data scarcity. We want to emphasize that the role of soil moisture can strongly affect the model solution. In the absence of reliable data, and to avoid introducing more complex uncertainties into this study, we chose this homogeneous approach.

[14] The radiative transfer scheme of Chen-Cotton [*Chen and Cotton*, 1983] was used to parameterize the vertical flux of shortwave and longwave radiation. Horizontal diffusion coefficients were computed on the basis of the modified Smagorinsky formulation [*Smagorinsky*, 1963], and the vertical diffusion was parameterized according to the Mellor-Yamada scheme [*Mellor and Yamada*, 1982]. The bulk microphysics parameterization was activated, which allows the model to consider the effect of moisture in all phases. The sea surface temperature was specified using the 1° monthly climatological data set from NCEP [*Reynolds and Smith*, 1994]. The convection scheme selected was the Kain-Fritsch scheme [*Kain and Fritsch*, 1993].

[15] In remote sensing, LST is defined as the "surface radiometric temperature" corresponding to the instantaneous field of view of the sensor [*Prata et al.*, 1995; *Becker and Li*, 1995]. RAMS does not output LST directly. In this study, canopy temperature and top layer soil temperature were combined to calculate LST in each grid cell on the basis of vegetation fractional cover (VFC), using the following equation:

$$LST^4 = \sigma_v T_v^4 + (1 - \sigma_v)T_g^4 \qquad (1)$$

where σ_V is VFC, T_V is the canopy temperature, and T_g is the top layer soil temperature [*Jin et al.*, 1997]. Temperatures here are in Kelvin.

2.2. Data

2.2.1. MODIS LAI and VFC

[16] Evaluation studies have shown that the accuracy of 8-day MODIS LAI is about 0.5 LAI [*Wang et al.*, 2004] and MODIS EVI performs with higher fidelity than AVHRR-NDVI by comparing with top-of-canopy and airborne measurements [*Huete et al.*, 2002]. Daily and 8-day MODIS products are often affected by cloud contaminations in tropical regions. Therefore, monthly 1 km MODIS LAI and EVI products for 2003, which were composited from

8-day data by selecting highest-quality pixels, were used in this study. They were downloaded from the MODIS group at Boston University (ftp://primavera.bu.edu/pub/datasets/MODIS/). These images were transformed to a Polar Stereographic projection, which corresponds to the projection of the RAMS domain. It needs to be mentioned that MODIS LAI has a meaning different than that in RAMS. As is standard in the remote sensing community, MODIS LAI is defined as "the area of green leaves per unit area of ground" [*Curran*, 1983; *Price*, 1992], which is sometimes referred to as "effective" LAI. In contrast, LAI in LEAF-2 and other land surface models is defined as "the number of leaf layers over the vegetated part of the pixel" (R. Dickinson, personal communication, 2006), which is also referred to as "clump" LAI [*Choudhury et al.*, 1994]. In each LEAF-2 patch, conservation equations for energy and moisture are applied to vegetation, canopy air and bare soil, and LAI is only assigned to the vegetated area [*Walko et al.*, 2000]. Therefore, MODIS LAI was divided by MODIS VFC so that the ingested LAI has the same meaning as defined in RAMS. This modification has the greatest influence on LAI values over sparsely vegetated areas where VFC is low. Further studies are needed to test the impacts of effective and modified LAI on model simulations.

[17] VFC data were developed from the 1 km monthly MODIS EVI product, based on the theory of "Mosaic Pixel," which assumes that a remote sensing pixel has a patchy (mosaic) structure [*Kerr et al.*, 1992; *Valor and Caselles*, 1996]. A quantity measured by satellite (ϕ, e.g., vegetation index) for a pixel can be interpreted as the sum of linear contributions from the vegetated area (σ_V) and bare soil $(1 - \sigma_V)$:

$$\phi = \phi_v \sigma_v + \phi_s(1 - \sigma_v) \qquad (2)$$

where the subscripts v and s denote values over fully vegetated and bare soil areas. A vegetation index is a proxy of vegetation density that is linearly related to fPAR and fractional vegetation cover. Various vegetation indices have also been shown to exponentially relate to the total green leaf area index. From this equation, a simple formulation for fractional cover σ_V can be derived as:

$$\sigma_v = \frac{\phi - \phi_s}{\phi_v - \phi_s} \qquad (3)$$

Following the study by *Gutman and Ignatov* [1998], ϕ_V and ϕ_S in this study are prescribed as seasonally and geographically invariant constants, which correspond to the yearly maximum EVI of the Congo Forest (approximately 0.86) and minimum EVI of deserts (approximately 0.05) in northern Kenya.

[18] Monthly MODIS LAI and VFC data were then directly ingested in RAMS. The 1 km LAI and VFC values were aggregated for each patch within a 50 km grid cell on the basis of land cover type. They were interpolated linearly to determine daily values so that RAMS can update LAI and VFC values continuously.

2.2.2. LAI and VFC Comparison

[19] In order to illustrate the improved representation of the land surface in the RAMS model, the default and new
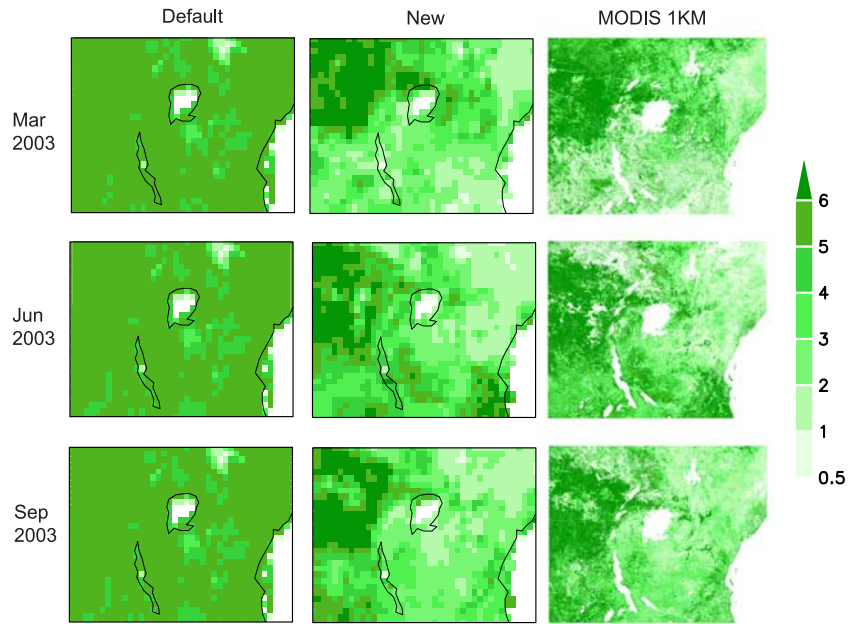
Figure 3. Spatial comparison of the default, new, and original 1 km LAI for March, June, and September 2003.

LAI and VFC were examined. Figures 3 and 4 present the spatial comparison of LAI and VFC respectively for different time periods in 2003: March, June, and September. The original 1 km MODIS imagery is also included in the comparison. The resolution for the default and new LAI and VFC maps is 50 km, which corresponds to the RAMS grid spacing (Figure 2). RAMS LAI and VFC values (default and new) shown in Figures 3 and 4 only represent the biggest patches in grid cells. As a result, details of smaller patches are not included and coastlines appear not explicitly resolved. Overall, the default LAI and VFC are extremely homogeneous spatially. Except for deserts and lakes, vegetation has little variation over the domain. The

default data show the Congo forest to have similar biophysical characteristics as the semiarid areas in the east. Furthermore, the default LAI and VFC present unrealistic temporal variation. For example, the observed VFC in a large part of southeast portion of the study area decreases significantly in the second half of the year. However, this is completely missed in the default VFC. In addition, seasonal variation of VFC was examined with detail for one land cover type (wooded grassland) at a selected location (8.9°S, 23.8°E) (Figure 5). Again, RAMS default VFC displayed little annual change and had much higher values compared to the MODIS observations. When daily or 8-day MODIS
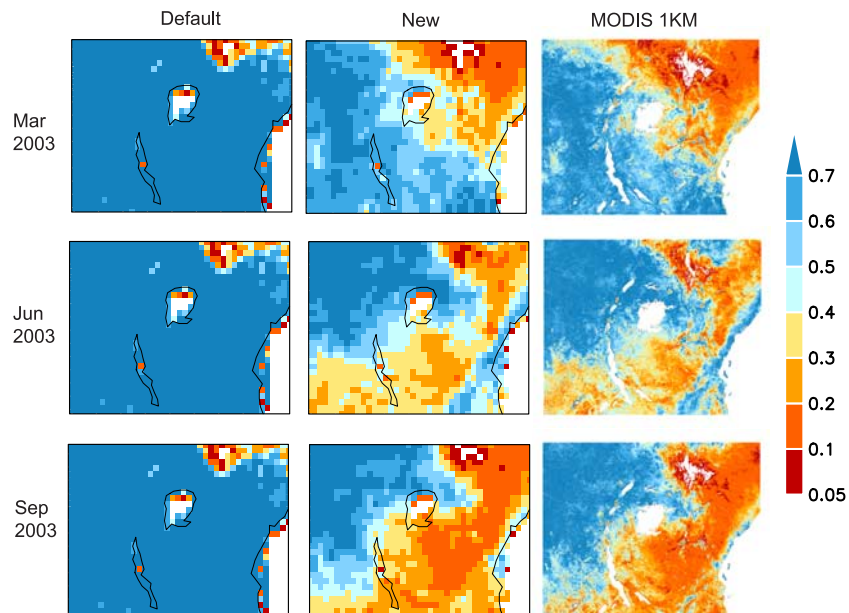
Figure 4. Same as in Figure 3 but for VFC.
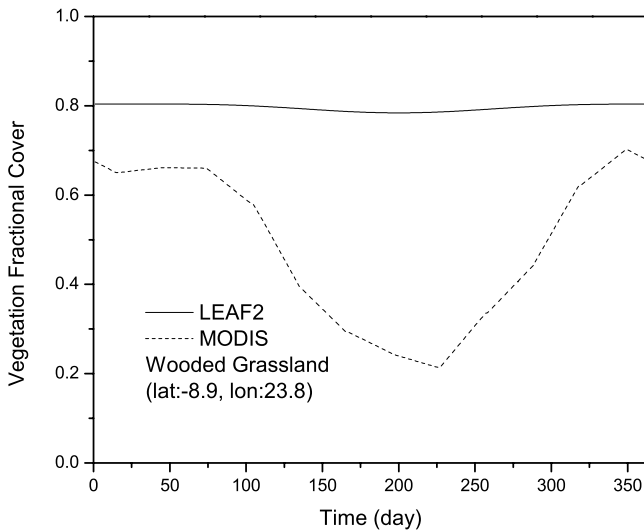
Figure 5. Seasonal variation of vegetation fractional cover for wooded grassland at one selected location.

vegetation products with high quality are available, the vegetation phenology could be further improved.

2.2.3. MODIS LST

[20] *Wan et al.* [2004] validated the daily MODIS LST product at 1 km resolution in 11 clear-sky cases with in situ measurement data and the accuracy was better than 1 K in the range from 263 to 300 K. However, no such validation has been reported for the East Africa region. Monthly Terra (MOD) and Aqua (MYD) LST data (version 4) with 0.05° (approximately 5.5 km) spatial resolution was downloaded from the EOS Data Gateway (http://wist.echo.nasa.gov). QC flags for quality assurance control were carefully examined with errors less than 3 K under clear sky conditions. Images were subset and resampled to 50 km footprint to match with RAMS output.

[21] It needs to be pointed out that MODIS LST is valid only under clear-sky conditions. For this low-latitude study
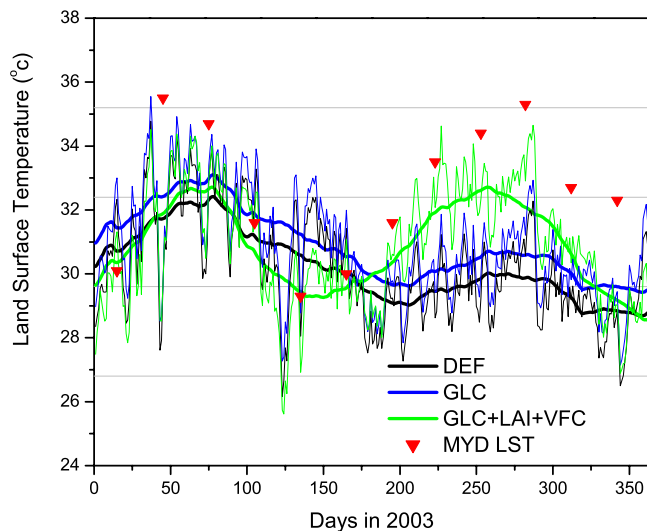
Figure 6. Temporal comparison of maximum daily LST from three RAMS runs (DEF, GLC, and GLC + LAI + VFC) and monthly MYD observations for the whole study domain.

Table 1. Data Quality of MODIS LST in 2003[a]

Month	MYD		MOD	
	Day	Night	Day	Night
1	O	X	O	O
2	O	O	O	O
3	O	O	O	X
4	O	O	O	O
5	O	O	O	O
6	O	O	O	O
7	O	O	O	O
8	O	O	O	O
9	O	X	O	O
10	O	X	O	X
11	O	X	O	X
12	O	X	O	X

[a]Circles indicate no significant cloud cover, and crosses indicate significant cloud contamination.

area, the daily product is usually severely contaminated by clouds. Monthly MODIS LST was thus used in this study. It was composited and averaged on the basis of clear-sky observations. However, LSTs in several months of 2003 were still adversely affected by the persistent cloud cover, especially over the western part of the study area (Congo forest) during nighttime. The data quality of MOD and MYD LST in 2003 based on cloud cover is summarized in Table 1, where circles indicate no significant cloud cover and crosses indicate significant cloud contamination. It is noticeable that most cloud contamination occurs during nighttime and in the raining seasons. Other factors such as algorithms and sensor characteristics could also affect the LST quality. The cloud cover, which produces invalid LST pixels, is the focus of this study.

[22] In this study, daytime MYD (1100 UTC or 1400 local time) was assumed as the maximum daily LST and was compared with RAMS LST at (1200 UTC) for the whole domain. Nighttime MYD (2300 UTC or 0200 local time) was assumed as the minimum daily LST, recognizing that minimum temperature may actually occur a couple of hours later in the early morning. Starting from 0000 UTC, RAMS yielded output at 3-h intervals. Thus, there is a 1 h difference between MOD and MYD observing times and the simulation times in RAMS. This difference may have some influence on the comparison in this study, which will be addressed in section 4. Since nighttime LST is usually contaminated with clouds in the western part of the domain, the minimum LST comparison was restricted to the eastern part of the domain. In addition, diurnal LST was compared from May to August, because of minimum cloud contamination in this time period (Table 1).

[23] In addition to the LST data, precipitation from the Tropical Rainfall Measuring Mission (TRMM) was also used for model evaluation [*Simpson et al.*, 1988; *Kummerow et al.*, 2000]. The TRMM products have recently been evaluated over East Africa using station observations [*Dinku et al.*, 2007], and they perform reasonably well. For this study, the latest TRMM product (3B42 version 6) was used.

3. Results

[24] Spatial, seasonal and diurnal LST was examined in three experiments (DEF, GLC and GLC + LAI + VFC) to look at the impacts of the ingested MODIS LAI and VFC. Precipitation was also examined.

Table 2. Mean, Standard Deviation, and Correlation Coefficient of LST Time Series in Figure 6 (Maximum) and Figure 7 (Minimum) Calculated on Monthly Averages[a]

Experiments	Maximum LST			Minimum LST		
	Mean (°C)	SD	Correlation Coefficient	Mean (°C)	SD	Correlation Coefficient
DEF	30.22	1.21	0.32	19.14	1.26	0.94
GLC	30.89	1.21	0.33	19.52	1.26	0.95
GLC + LAI + VFC	30.91	1.51	0.86	19.42	1.11	0.90
MYD	32.58	2.14	–	18.01	1.23	–

[a]Correlation coefficients are between three experiments and MODIS observations (MYD). SD stands for standard deviation.

3.1. Seasonal LST

[25] Figure 6 shows the RAMS simulated maximum daily LSTs and the MYD monthly composited observations, which were averaged for the whole study area excluding water bodies. The three runs are differentiated in colors and bold lines are simply 30-day averages of daily results. Detailed statistics of each time series are given in Table 2. The impacts of the land surface conditions are significant, especially when MODIS LAI and VFC products were used. In contrast with the RAMS default land surface, LST seasonal variation has been dramatically improved in GLC + LAI + VFC (green curve in Figure 6). According to MYD observations the lowest LST in 2003 occurs in May. This is correctly captured by GLC + LAI + VFC, but is incorrectly simulated to be in July by DEF and GLC runs. The improved seasonality is also shown by standard deviation and correlation coefficients in Table 2. GLC + LAI + VFC increases seasonal LST variation (standard deviation) with substantially improved correlation (0.86) with MYD observations. LSTs peak at about the same time periods (March and September) in all three runs. However, RAMS underestimates LST in the second half of the year. Overall, GLC2000 increases the maximum daily LST by about half degree (Table 2), but fails to change the seasonal dynamics. LST flattens out later in the year, both with and without GLC2000. The increase in LST in the second half of the year, giving better agreement with observations, is due to more realistic description of vegetation cover in GLC + LAI + VFC, particularly seasonal phenology of VFC, which will be analyzed with detail in section 4.

[26] Minimum daily LST is also compared in Figure 7. Because a significant amount of invalid LST pixels exist in the nighttime MYD in the western domain from September to January (Table 1), this comparison was conducted only for the eastern domain, which is approximately the eastern half of the study area. Water bodies were excluded in this comparison as well. Detailed statistics of each time series are given in Table 2. Generally, RAMS produces much better minimum LST dynamics than the maximum LST in all three runs. This is possibly due to less moisture in this arid/semiarid area. Unlike the maximum daily LST, the lowest minimum LST occurs in July. Seasonal variation is as large as about four degrees. Similarly as in Figure 6, RAMS produces lower LSTs at the beginning of the year, but higher LSTs after June using the GLC + LAI + VFC run. In addition, GLC2000 does not have much impact on the LST seasonality. Table 2 (mean LST) indicates that RAMS shows a warm bias at night but a cold bias during the day. This is possibly related to the characteristics of MODIS products and other factors that will be discussed in detail in section 4.

3.2. Spatial LST

[27] In Figure 8, the maximum daily LSTs from MODIS (MYD daytime) and RAMS are spatially compared month by month. The first image for each month is from the MODIS observations, resampled to 50 km resolution. Only LSTs from the DEF run (second image) and the GLC + LAI + VFC run (third image) are included. Because the comparison is in terms of land surface temperature all water bodies (lakes and oceans) were masked out (white color). The magnitude of LST is indicated by color: yellow to red show high LSTs while green to blue show relatively low LSTs.

[28] MODIS LSTs peak from February to March and again from August to September, and reach their minimum around May. This is consistent with the bimodal temporal pattern shown in Figure 6. This feature is obviously captured by the GLC + LAI + VFC run, but is completely missed by the DEF run. LSTs do not vary much after June for the DEF run. Spatially, the western domain which is covered by more vegetation and has more moisture and rainfall has lower LSTs compared to the eastern part. Both the DEF and the GLC + LAI + VFC runs seem to capture this feature, but the latter captures this contrast much better. More importantly, MODIS-observed LSTs in the east shows a strong Intertropical Convergence Zone (ITCZ) related pattern, in which hottest LSTs migrate from north to south with time and correspond to the local dry season. This feature is fully captured by the GLC + LAI + VFC run. In Figure 4, the MODIS VFC shows a similar pattern. This
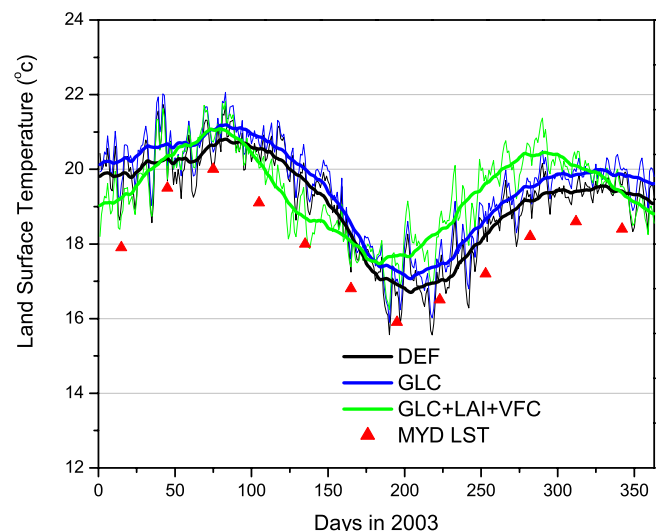
Figure 7.   Same as in Figure 6 but for minimum daily LST and for eastern domain only.
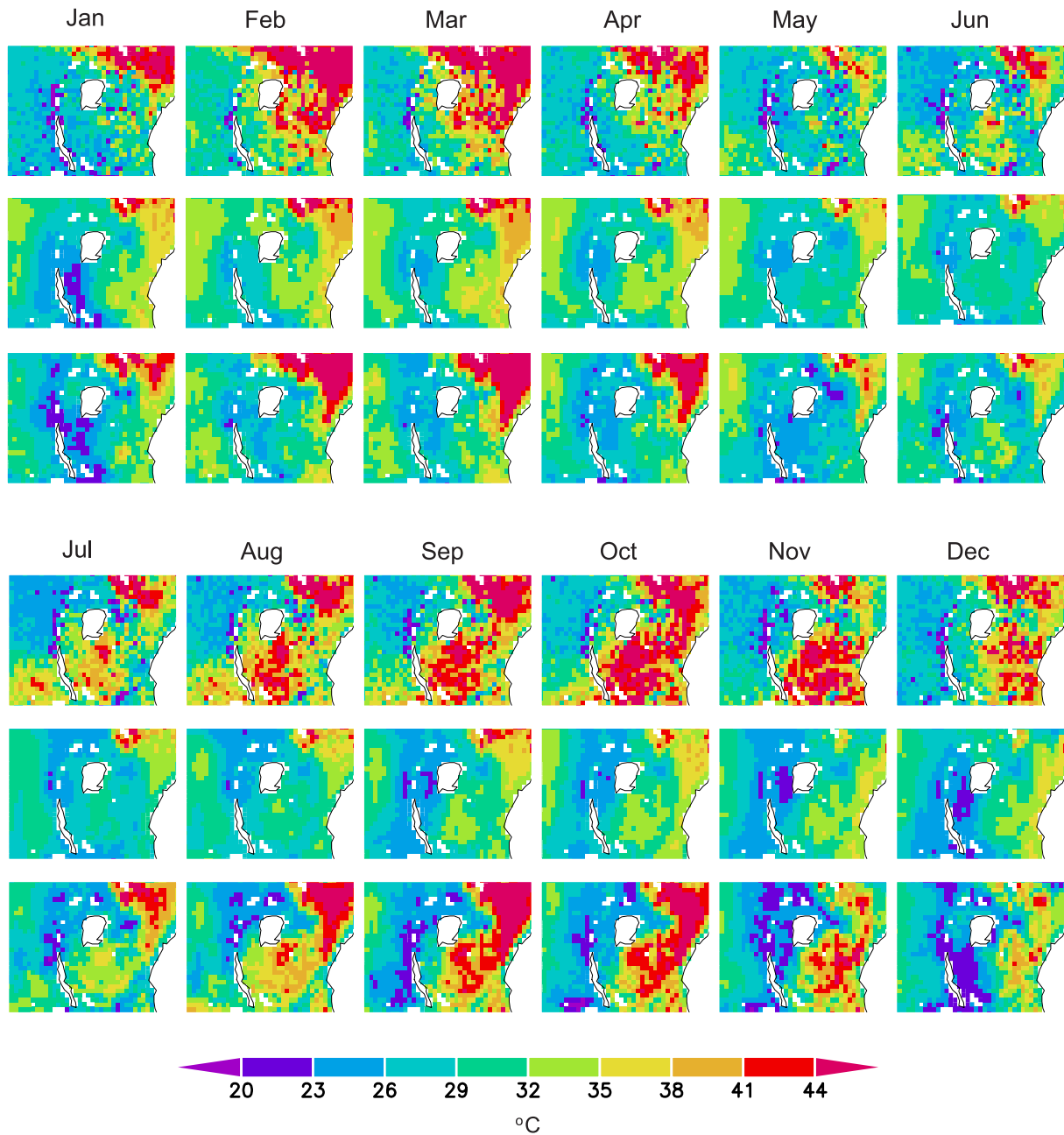
Figure 8. Spatial comparison of LST from MODIS observations (first image for each month), RAMS with default land cover and biophysical parameters, DEF run (second image for each month), and RAMS with GLC2000 and MODIS LAI/VFC, GLC + LAI + VFC run (third image for each month).

confirms the importance of VFC in calculating LST as is manifested in equation (1). The warmer bare soil temperatures gain more importance during the July–August or so time period because of the low VFC that is manifested only in the MODIS-driven experiment. Maximum, minimum and standard deviation of LST in each panel in Figure 8 are given in Table 3. Seasonal variation of these three statistics follows the similar pattern in Figure 6. Table 3 also indicates a cold daytime bias in RAMS.

[29] In addition to the month-by-month examination of MYD and simulated spatial LSTs, differences between them are presented in Figure 9. LST differences are averaged over two periods: January to June and July to December 2003.

Similar to Figure 8, the biggest differences occur in the eastern domain primarily showing a cold bias in RAMS. In the western domain (mostly Congo forest area), RAMS produces higher LSTs. Averaged over the first half year, DEF performs a little better than GLC + LAI + VFC run in terms of mean (mn) LST difference. However, during the second half, LST from the GLC + LAI + VFC run becomes much closer to observations.

3.3. Diurnal LST

[30] The impacts of the land surface representation in RAMS were further examined by looking at diurnal LSTs, taking advantage of the multiple daily observations by

Table 3. Maximum, Minimum, and Standard Deviation of LST for Panels in Figure 8[a]

Months	Maximum			Minimum			SD		
	MYD	DEF	GLV	MYD	DEF	GLV	MYD	DEF	GLV
1	55.8	46.2	52.2	16.3	22.2	21.0	6.7	4.7	5.4
2	57.6	49.9	56.1	18.5	23.2	21.4	7.7	4.3	6.7
3	57.5	50.0	57.0	19.9	23.7	21.9	7.9	4.5	7.3
4	56.0	47.6	53.4	17.5	23.1	20.7	6.4	4.1	5.9
5	49.4	44.7	48.3	10.0	23.3	18.5	4.3	3.4	4.3
6	50.6	45.7	49.3	16.2	22.8	18.0	5.4	3.1	3.8
7	51.3	46.0	52.0	11.4	22.2	19.7	6.3	3.4	5.3
8	52.1	45.3	52.2	13.7	22.1	21.1	7.0	3.6	6.6
9	54.5	48.0	54.6	11.2	21.7	20.0	7.4	4.4	8.0
10	55.5	44.9	50.2	13.1	22.3	19.2	7.6	4.0	7.7
11	53.4	42.4	47.7	16.4	21.8	19.9	7.2	3.7	6.4
12	55.4	43.8	44.6	14.3	21.8	20.1	6.9	3.8	5.1

[a]GLV stands for GLC + LAI + VFC. Unit is °C.

MODIS Terra (MOD) and MODIS Aqua (MYD). Because of cloud contamination (Table 1), only four months, May to August, were analyzed. In Figure 10, the RAMS simulated LSTs are shown by the color lines, while the four MODIS observations are shown in red squares. Time is in UTC, which lags local time about 3 h in the study area. Mean LST and diurnal temperature range are given in Table 4.

[31] Figure 10 shows that RAMS captures the diurnal cycles quite well. LST reaches its daily maximum at about 1200 UTC and the daily minimum at about 0300 UTC. During the day (0900 and 1200 UTC), the simulated LST is close to the MODIS values in May and June. However, in July and August the differences between simulated and observed daytime LSTs magnify. This is also shown in Figure 6. During the day in July and August, only the LSTs simulated by the GLC + LAI + VFC run are close to the

MODIS observations. In Table 4, diurnal temperature range calculated by GLC + LAI + VFC increases significantly with time which is consistent with MODIS observations. In general, the GLC + LAI + VFC produces the coldest LST in May and June but the warmest LST in July and August (Table 4). This is because the vegetation cover as well as soil moisture decreases dramatically during this time period (dry season) in larger part of the domain (Figure 4), which inhibits transpiration (more discussion to follow in section 4).

3.4. Precipitation

[32] Figure 11 shows the TRMM-observed 3-h precipitation rates in 2003. The TRMM observations are compared with the three RAMS simulations: DEF, GLC, and GLC + LAI + VFC. RAMS is able to produce the general temporal dynamics of rainfall in this area considering RAMS has a much lower spatial footprint size than the TRMM observations (50 km versus about 27 km). The two wet seasons separated by a dry season in between (around June) are clearly captured. In contrast to LST, the RAMS simulated precipitation seems to be less sensitive to different land surface representations. All three experiments produced similar rainfall patterns. In Figure 11, mean precipitation rates are 0.098, 0.088, 0.093 and 0.091 mm/3 h for TRMM, DEF, GLC and GLC + LAI + VFC, respectively. An one-way analysis of variance (ANOVA) test showed no difference at the 95% significance level among three time series in Figure 11 (DEF, GLC and GLC + LAI + VFC). The p value of this test was 0.196. Figure 12 shows the accumulated precipitation over the domain for 2003. Spatially, the major features are captured by RAMS, such as high rainfall over the Congo forest and Lake Victoria and relatively dry areas in eastern Kenya and Tanzania. However, RAMS
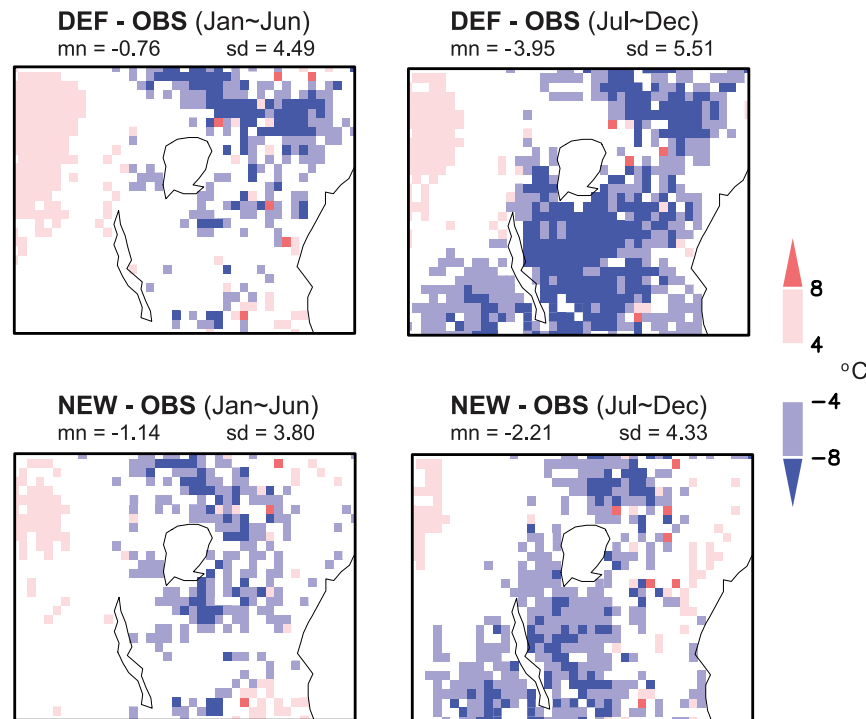
Figure 9. Spatial differences between MYD LST (OBS) and simulated LSTs averaged over January–June 2003 and July–December 2003. NEW means the GLC + LAI + VFC run. The mean (mn) and standard deviation (sd) for each panel are also given.
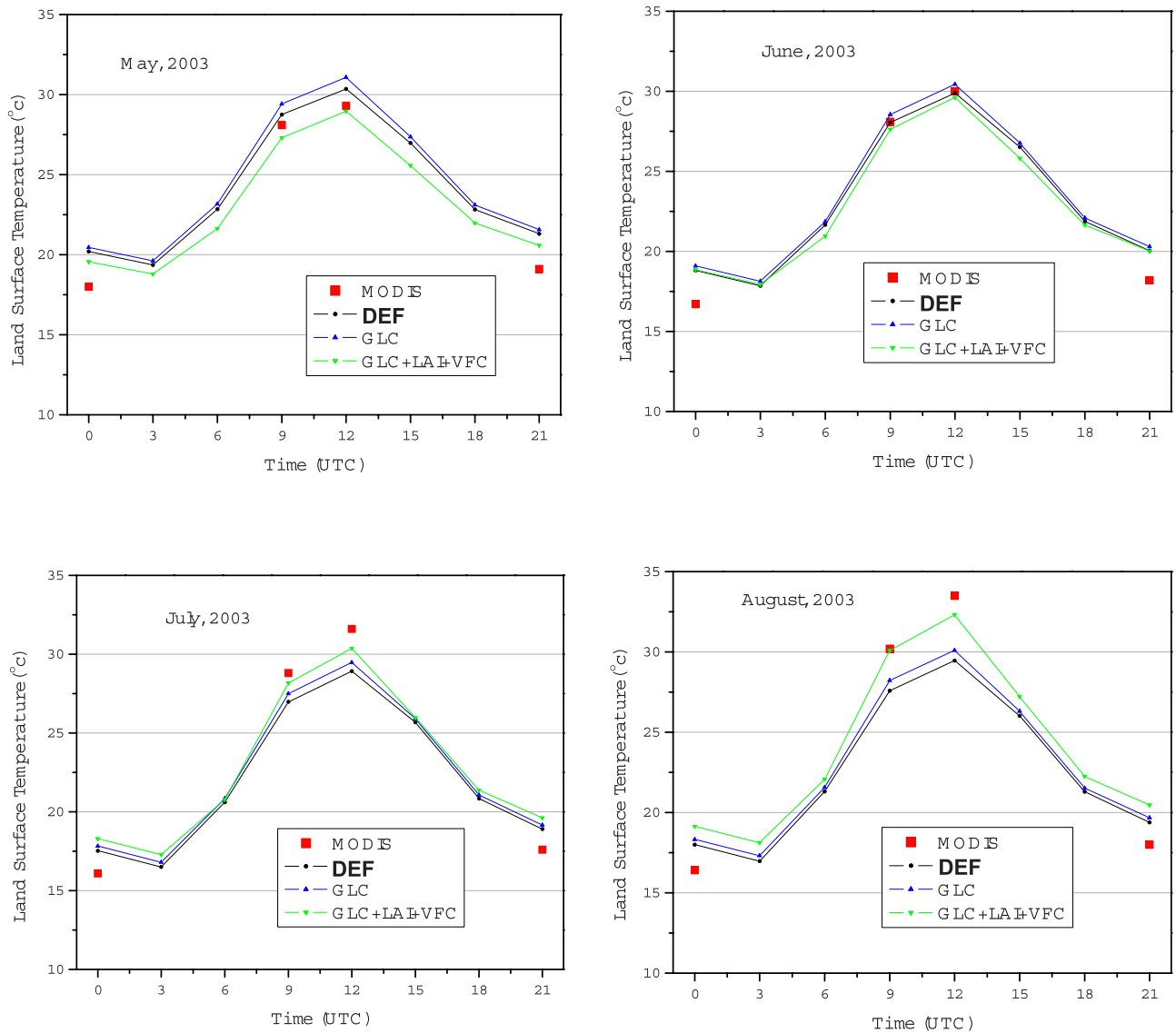
Figure 10. Monthly averaged diurnal cycles from MODIS and three RAMS runs: DEF, GLC, and GLC + LAI + VFC.

produces little rainfall at the left and right boundaries and much more rainfall over Congo forest than observations. Although there are some differences in terms of mean values and standard deviations as well as over hot spot areas (e.g., high rainfall area), different surface conditions in DEF, GLC and GLC + LAI + VFC have little impacts on the overall precipitation pattern.

4. Discussion

[33] The partitioning of sensible and latent heat flux is a function of varying surface soil water content and vegetation cover. Since vegetation considerably enhances water vapor fluxes to the atmosphere through the transpiration process, greater vegetation cover is often associated with increased latent heat losses and therefore a reduction in surface temperature. Increasing vegetation height increases surface roughness, turbulent exchange of water above the canopy, and the efficiency of energy dissipation. It thus further

decreases surface temperature [*Smith and Choudhury*, 1990]. In addition, during daylight hours, plant leaves are cooler than exposed bare soil because the heat capacity of plant leaves is much lower than the heat capacity of soil [*Gates*, 1980]. On surface with a low moisture content, latent heat fluxes associated with evaporation and transpiration become the dominant mechanism accounting for variations

Table 4. Mean LST and Diurnal Temperature Range for Monthly Averaged Diurnal Cycles in Figure 10[a]

	Mean				DTR			
Months	MODIS	DEF	GLC	GLV	MODIS	DEF	GLC	GLV
5	23.6	24.1	24.5	23.1	11.3	11.0	11.5	10.2
6	23.3	23.1	23.4	22.8	13.3	12.0	12.3	11.7
7	23.5	22.0	22.3	22.7	15.5	12.4	12.7	13.1
8	24.5	22.5	22.9	24.0	17.1	12.5	12.8	14.2

[a]GLV stands for GLC + LAI + VFC. DTR stands for diurnal temperature range. Unit is °C.
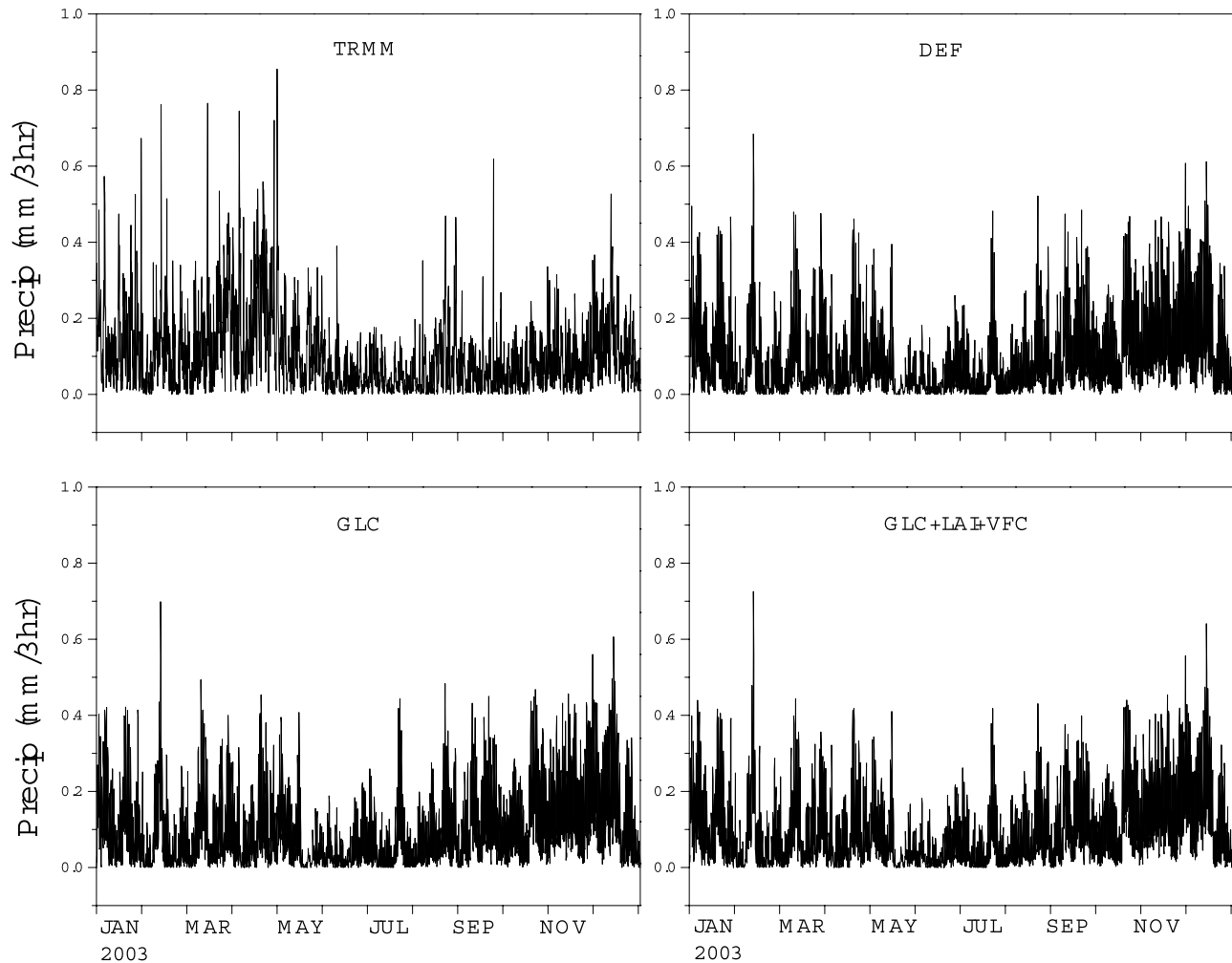
Figure 11. Domain averaged 3-h precipitation rate from TRMM for 2003 and three RAMS runs: DEF, GLC, and GLC + LAI + VFC.

in surface temperature with increases in vegetation cover [*Price*, 1990].

[34] As shown in Figure 9, the greatest LST difference found in this study occurs in the eastern domain, which is a primarily semiarid area with limited soil moisture. By incorporating spatially and temporally explicit MODIS LAI and VFC, RAMS improved its performance of simulating the seasonal dynamics of LST in two ways. Informed by the MODIS LAI data, a more realistic vegetation density of the vegetated area in a grid cell may help to improve the interactions of plants and overlying atmosphere. The other one, which is more important, is the relative contributions of vegetation and bare soil as determined by VFC. Significantly increased spatial extent of bare soil in the eastern domain during the second half of the year (Figure 4) may help to lift the flat LST curves after June (Figure 6). MODIS VFC provides more realistic description of the less vegetated zone in the eastern domain during the later part of the year, which has much less physical evaporation and transpiration. The surface temperature in GLC + LAI + VFC therefore increases compared to DEF and GLC with unrealistically complete coverage by vegetation.

[35] As discussed in section 2.1, the land surface in RAMS is primarily represented by both land cover types and their related biophysical parameters. Introducing a new land cover data set, GLC2000, provides a better description of the spatial distribution of land cover types across the study domain. This should help to produce better spatial characteristics of LST. However, GLC2000 did not result in improvement in seasonal vegetation dynamics, which are still prescribed as simple mathematical equations in LEAF-2. The temperatures of vegetation and bare soil, as well as their relative contributions in a grid cell (equation (1)), vary not just by location, but also over time. As a result, using GLC2000 alone does not improve the LST seasonality.

[36] Climate is a major determinant of vegetation. The location and seasonal migration of ITCZ are crucial for large areas of the tropics including East Africa. It links to the rainy season, which supplies a large fraction of the annual rainfall. We can trace a causal continuum wherein ITCZ leads to rainfall patterns that determine vegetation distribution and structure that affect the spatial and temporal characteristics of LST. In this study, a large area south of Lake Victoria is in the Southern Hemisphere (Figure 2). From April to September the vertical rays of the Sun strike
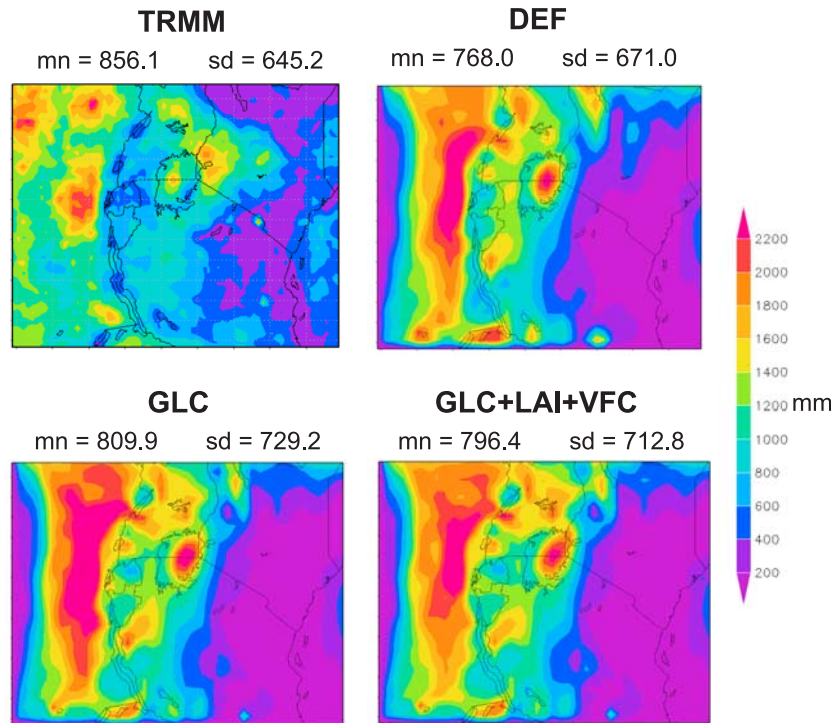
Figure 12. Accumulated precipitation in 2003 from TRMM and three RAMS runs: DEF, GLC, and GLC + LAI + VFC. The mean (mn) and standard deviation for each plot are also given.

the Earth's surface north of the equator, and therefore the area south of Lake Victoria receives less insolation. MODIS observations (Figure 8), however, show that LST over this area starts to increase during this time period. In contrast, the area south of Lake Victoria receives more insolation during October to March, and the LST decreases with time. The spatial pattern of LST is primarily related to the movement of ITCZ. From April to September, ITCZ moves toward the Northern Hemisphere, which leads to less rainfall with sparser vegetation in the area south of Lake Victoria, which in turn contributes to higher LST. The causal continuum can also be applied to the period from October to March. This study demonstrates (section 3.2) that MODIS LAI and VFC significantly enhance the ITCZ-related pattern of LST compared to the default vegetation conditions.

[37] Precipitation in RAMS is governed by large-scale fields and model parameterizations. In this study, the demonstrated improvement of the land surface representation is not sufficient to change the simulated precipitation significantly. This is probably due to the 50 km horizontal grid spacing used for RAMS. Reducing the grid spacing may better represent the mesoscale structure of precipitation. The Kain-Fritsch convection scheme, which has been suggested to be more suitable for modeling with ∼30 km grid spacing [*Kain and Fritsch*, 1993], was used in this study. Additionally, the greatest difference in vegetation cover between MODIS observations and RAMS default conditions occurs in considerably dry areas (Figure 4), which may also influence the sensitivity of precipitation to land surface conditions.

[38] RAMS showed a notable warm bias at night and a cold bias during the day (Table 2). Three possible factors

may contribute to this in the model. The first factor is related to the LST product itself. Monthly MODIS LST is composited on the basis of clear-sky observations. By screening out cloud contamination, the MODIS observations are biased toward the highest daytime values and the lowest nighttime values in a month. In the daytime, clouds diminish insolation and thus cause much lower LSTs; during the night, clouds tend to keep surface warmer by absorbing and emitting longwave radiation from the Earth. The second factor involves the lag of about 1 h between MODIS observation times and RAMS simulation times. According to the study by *Jin and Dickinson* [1999], the timing of maximum LST corresponds to the insolation peak time, with some phase lag. LST may begin to decrease after 1400 local time (MYD). Using 1500 local time RAMS simulation time for comparing maximum LST could be a factor in the cold bias shown in previous results. The final factor is soil moisture, which was not validated in the model. Excessive soil moisture in the semiarid area (eastern domain) may reduce the simulated LST because of the latent heat flux.

5. Summary

[39] Human activities have substantially modified the Earth's surface in the past and will continue to do so in the future. The impacts of human activities such as land cover change on regional and global climate can be studied using climate modeling techniques. Two types of data are required for effective land-climate modeling studies. One is biophysical variables used in the land surface parameterization, and the other is the climatic variables for validating model outputs. However, these data are usually limited in

many parts of the world such as East Africa in this study. This brings formidable challenges for land-climate modeling studies in those areas.

[40] In this paper, MODIS LAI and VFC images were directly incorporated in the RAMS model. Spatially, the default LAI and VFC were too homogeneous to differentiate distinct land surface types across the domain. Temporally, simple cosine functions of very small magnitude and a phase appropriate to midlatitudes produced unrealistic seasonal variation in East Africa. The impacts of this improved land surface were examined by comparing the RAMS simulated LST and LST products from both MODIS Terra and Aqua satellites. The spatial, seasonal and diurnal LST characteristics were greatly improved because of the ingested MODIS LAI and VFC. The bimodal feature of the LST seasonal variation, which was completely missed in the default configurations, was captured when MODIS LAI and VFC were used. The ITCZ-related seasonal migration of LST in the eastern domain was also greatly enhanced. Both MODIS Terra and Aqua LST were used for the first time to validate the diurnal pattern of model outputs. This study found that diurnal LST cycles were slightly improved because of the new land surface representation. GLC2000 alone, however, was not able to modify the seasonality of LST. Precipitation was less sensitive to the change in the land surface conditions primarily because of model configuration and the convection scheme used. Vegetation changes in arid areas may also contribute to this insensitivity.

[41] EOS satellites are providing a new generation of land data products in support of global change research and natural resource management. However, it usually takes time for new land products derived from a new sensor system to be adopted by users. As with AVHRR in the past, the potential of EOS products has not been fully recognized in the climate modeling community. This paper presents the use of EOS products to improve the land-climate modeling in East Africa. More EOS products need to be tested in the land-climate modeling studies at regional and global scales.

References

Becker, F., and Z.-L. Li (1995), Surface temperature and emissivity at different scales: Definition, measurement and related problems, *Remote Sens. Rev.*, *12*, 225–253.

Castro, C. L., R. A. Pielke Sr., and G. Leoncini (2005), Dynamical downscaling: Assessment of value retained and added using the Regional Atmospheric Modeling System, *J. Geophys. Res.*, *110*, D05108, doi:10.1029/2004JD004721.

Chase, T. N., R. A. Pielke Sr., T. G. F. Kittel, J. S. Baron, and T. J. Stohlgren (1999), Potential impacts on Colorado Rocky Mountain weather and climate due to land use changes on the adjacent Great Plains, *J. Geophys. Res.*, *104*, 16,673–16,690, doi:10.1029/1999JD900118.

Chase, T. N., R. A. Pielke Sr., T. G. F. Kittel, R. Nemani, and S. W. Running (2000), Simulated impacts of historical land cover changes on global climate in northern winter, *Clim. Dyn.*, *16*, 93–105, doi:10.1007/s003820050007.

Chen, C., and W. R. Cotton (1983), A one-dimensional simulation of the stratocumulus-capped mixed layer, *Boundary Layer Meteorol.*, *25*, 289–321, doi:10.1007/BF00119541.

Choudhury, B. J., et al. (1994), Relations between evaporation coefficients and vegetation indices studied by model simulations, *Remote Sens. Environ.*, *50*, 1–17, doi:10.1016/0034-4257(94)90090-6.

Cotton, W. R., et al. (2003), RAMS 2001: Current status and future directions, *Meteorol. Atmos. Phys.*, *82*, 5–29, doi:10.1007/s00703-001-0584-9.

Crawford, T. M., et al. (2001), Value of incorporating satellite-derived land cover data in MM5/PLACE for simulating surface temperatures, *J. Hydrometeorol.*, *2*, 453–468, doi:10.1175/1525-7541(2001)002<0453:VOISDL>2.0.CO;2.

Curran, P. J. (1983), Multispectral remote sensing for the estimation of green leaf area index, *Philos. Trans. R. Soc. London*, *309*, 257–270, doi:10.1098/rsta.1983.0039.

Deardorff, J. W. (1978), Efficient prediction of ground surface temperature and moisture, with inclusion of layer of vegetation, *J. Geophys. Res.*, *83*, 1889–1903, doi:10.1029/JC083iC04p01889.

de Foy, B., L. T. Molina, and M. J. Molina (2006), Satellite-derived land surface parameters for mesoscale modelling of the Mexico City basin, *Atmos. Chem. Phys.*, *6*, 1315–1330.

DeFries, R. S., L. Bounoua, and G. J. Collatz (2002), Human modification of the landscape and surface climate in the next fifty years, *Global Change Biol.*, *8*, 438–458, doi:10.1046/j.1365-2486.2002.00483.x.

Dickinson, R. E. (1995), Land processes in climate models, *Remote Sens. Environ.*, *51*, 27–38, doi:10.1016/0034-4257(94)00062-R.

Dickinson, R. E., A. Henderson-Sellers, P. J. Kennedy, and M. F. Wilson (1986), Biosphere-atmosphere transfer scheme for the NCAR community climate model, *NCAR Tech. Note, NCAR/TN-275+STR*, Natl. Cent. for Atmos. Res., Boulder, Colo.

Dickinson, R. E., A. Henderson-Sellers, C. Rosenzweig, and P. J. Sellers (1991), Evapotranspiration models with canopy resistance for use in climate models, a review, *Agric. For. Meteorol.*, *54*, 373–388, doi:10.1016/0168-1923(91)90014-H.

Dinku, T., P. Ceccato, E. Grover-Kopec, M. Lemma, S. J. Connor, and C. F. Ropelewski (2007), Validation of satellite rainfall products over East Africa's complex topography, *Int. J. Remote Sens.*, *28*, 1503–1526.

Feddema, J. J., K. W. Oleson, G. B. Bonan, L. O. Mearns, L. E. Buja, G. A. Meehl, and W. M. Washington (2005), The importance of land-cover change in simulating future climates, *Science*, *310*, 1674–1678, doi:10.1126/science.1118160.

Friedl, M. A., et al. (2002), Global land cover mapping from MODIS: Algorithms and early results, *Remote Sens. Environ.*, *83*, 287–302, doi:10.1016/S0034-4257(02)00078-0.

Gates, D. M. (1980), *Biophysical Ecology*, Springer, New York.

Ge, J. (2007), Improving regional climate modeling in East Africa using remote sensing products, Ph.D. dissertation, Mich. State Univ., East Lansing.

Ge, J., J. Qi, B. M. Lofgren, N. Moore, N. Torbick, and J. M. Olson (2007), Impacts of land/use cover classification accuracy on regional climate simulations, *J. Geophys. Res.*, *112*, D05107, doi:10.1029/2006JD007404.

Giorgi, F., and L. O. Mearns (1999), Introduction to special section: Regional climate modeling revisited, *J. Geophys. Res.*, *104*, 6335–6352, doi:10.1029/98JD02072.

Gutman, G., and A. Ignatov (1998), The deviation of the green vegetation fraction from NOAA/AVHRR data for use in numerical weather prediction models, *Int. J. Remote Sens.*, *19*, 1533–1543, doi:10.1080/014311698215333.

Houghton, R. A., J. L. Hackler, and K. T. Lawrence (1999), The U.S. carbon budget: Contributions from land-use change, *Science*, *285*, 574–578, doi:10.1126/science.285.5427.574.

Huete, A., et al. (2002), Overview of the radiometric and biophysical performance of the MODIS vegetation indices, *Remote Sens. Environ.*, *83*, 195–213, doi:10.1016/S0034-4257(02)00096-2.

International Geosphere-Biosphere Programme (1990), The International Geosphere-Biosphere Programme: A study of global change—The initial core projects, *IGBP Rep. 12*, Stockholm, Sweden.

Intergovernmental Panel on Climate Change (2000), Summary for policy makers, in *IPCC Special Report on Land Use, Land-Use Change, and Forestry* [electronic], Geneva, Switzerland.

Jacob, D., and R. Podzun (1997), Sensitivity studies with the regional climate model REMO, *Meteorol. Atmos. Phys.*, *63*, 119–129, doi:10.1007/BF01025368.

Jin, M., and R. E. Dickinson (1999), Interpolation of surface radiative temperature measured from polar orbiting satellites to a diurnal cycle: 1. Without clouds, *J. Geophys. Res.*, *104*, 2105–2116, doi:10.1029/1998JD200005.

Jin, M., R. E. Dickinson, and A. M. Vogelmann (1997), A comparison of CCM2-BATS skin temperature and surface-air temperature with satellite and surface observations, *J. Clim.*, *10*, 1505–1524, doi:10.1175/1520-0442(1997)010<1505:ACOCBS>2.0.CO;2.

Justice, C. O., et al. (2002), An overview of MODIS land data processing and product status, *Remote Sens. Environ.*, *83*, 3–15, doi:10.1016/S0034-4257(02)00084-6.

Kain, J. S., and J. M. Fritsch (1993), Convective parameterization for mesoscale models: The Kain-Fritsch scheme, in *The Representation of Cumulus Convection in Numerical Models*, *Meteorol. Monogr.*, 24, 165–170.

Kalnay, E., et al. (1996), The NCEP/NCAR 40-year reanalysis project, *Bull. Am. Meteorol. Soc.*, 77, 437–471, doi:10.1175/1520-;0477(1996)077<0437:TNYRP>2.0.CO;2.

Kerr, Y. H., J. P. Lagouarde, and J. Imbernon (1992), Accurate land surface temperature retrieval from AVHRR data with use of an improved split-window algorithm, *Remote Sens. Environ.*, 41, 197–209, doi:10.1016/0034-4257(92)90078-X.

Kummerow, C., et al. (2000), The status of the tropical rainfall measuring mission (TRMM) after two years in orbit, *J. Appl. Meteorol.*, 39, 1965–1982, doi:10.1175/1520-0450(2001)040<1965:TSOTTR>2.0.CO;2.

Kurkowski, N. P., D. J. Stensrud, and M. E. Baldwin (2003), Assessment of implementing satellite-derived land cover data in the Eta model, *Weather Forecast.*, 18, 404–416, doi:10.1175/1520-0434(2003)18<404:AOISDL>2.0.CO;2.

Lee, T. J. (1992), The impact of vegetation on the atmospheric boundary layer and convective storms, *Atmos. Sci. Pap. 509*, Colorado State Univ., Fort Collins.

Lu, L., and W. J. Shuttleworth (2002), Incorporating NDVI-derived LAI into the climate version of RAMS and its impact on regional climate, *J. Hydrometeorol.*, 3, 347–362, doi:10.1175/1525-7541(2002)003<0347:INDLIT>2.0.CO;2.

Lu, L., et al. (2001), The implementation of a two-way interactive atmospheric and ecological model and its application to the central United States, *J. Clim.*, 14, 900–919, doi:10.1175/1520-0442(2001)014<0900:IOATWI>2.0.CO;2.

Mayaux, P., E. Bartholomé, S. Fritz, and A. Belward (2004), A new land-cover map of Africa for the year 2000, *J. Biogeogr.*, 31, 861–877, doi:10.1111/j.1365-2699.2004.01073.x.

Mellor, G. L., and T. Yamada (1982), Development of a turbulence closure model for geophysical fluid problems, *Rev. Geophys.*, 20, 851–875, doi:10.1029/RG020i004p00851.

Mukabana, J. R., and R. A. Pielke Sr. (1996), Investigating the influence of synoptic-scale monsoonal winds and mesocale circulations on diurnal weather patterns over Kenya using a mesoscale numerical model, *Mon. Weather Rev.*, 124, 224–243, doi:10.1175/1520-0493(1996)124<0224:ITIOSS>2.0.CO;2.

Pielke, R. A., Sr. (1992), A comprehensive meteorological modeling system—RAMS, *Meteorol. Atmos. Phys.*, 49, 69–91, doi:10.1007/BF01025401.

Pielke, R. A., Sr., R. L. Walko, L. T. Steyaert, P. L. Vidale, G. E. Liston, W. A. Lyons, and T. N. Chase (1999), The influence of anthropogenic landscape changes on weather in south Florida, *Mon. Weather Rev.*, 127, 1663–1673, doi:10.1175/1520-0493(1999)127<1663:TIOALC>2.0.CO;2.

Pielke, R. A., Sr., et al. (2002), The influence of land-use change and landscape dynamics on the climate system: Relevance to climate-change policy beyond the radiative effect of greenhouse gases, *Philos. Trans. R. Soc. London, Ser. A*, 360, 1705–1719, doi:10.1098/rsta.2002.1027.

Pitman, A. J. (2003), The evolution of, and revolution in, land surface schemes designed for climate models, *Int. J. Climatol.*, 23, 479–510, doi:10.1002/joc.893.

Prata, A. J., et al. (1995), Thermal remote sensing of land surface temperature from satellites: Current status and future prospects, *Remote Sens. Rev.*, 12, 175–224.

Price, J. C. (1990), Using spatial context in satellite data to infer regional scale evapotranspiration, *IEEE Trans. Geosci. Remote Sens.*, 28, 940–948, doi:10.1109/36.58983.

Price, J. C. (1992), Estimating vegetation amount from visible and near-infrared reflectances, *Remote Sens. Environ.*, 41, 29–34, doi:10.1016/0034-4257(92)90058-R.

Reynolds, R. W., and T. M. Smith (1994), Improved global sea surface temperature analyses using optimum interpolation, *J. Clim.*, 7, 929–948, doi:10.1175/1520-0442(1994)007<0929:IGSSTA>2.0.CO;2.

Santanello, J. A., and T. N. Carlson (2001), Mesoscale simulation of rapid soil drying and its implication for predicting daytime temperature, *J. Hydrometeorol.*, 2, 71–88, doi:10.1175/1525-7541(2001)002<0071:MSORSD>2.0.CO;2.

Sellers, P. J., D. A. Randall, G. J. Collatz, J. A. Berry, C. B. Field, D. A. Dazlich, C. Zhang, G. D. Collelo, and L. Bounoua (1996a), A revised land surface parameterization (SiB2) for atmospheric GCMs. Part 1: Model formulation, *J. Clim.*, 9, 676–705, doi:10.1175/1520-0442(1996)009<0676:ARLSPF>2.0.CO;2.

Sellers, P. J., S. O. Los, C. J. Tucker, C. O. Justice, D. A. Dazlich, G. J. Collatz, and D. A. Randall (1996b), A revised land surface parameterization (SiB2) for atmospheric GCMs. Part 2: The generation of global fields of terrestrial biophysical parameters from satellite data, *J. Clim.*, 9, 706–737, doi:10.1175/1520-0442(1996)009<0706:ARLSPF>2.0.CO;2.

Sellers, P. J., et al. (1997), Modeling the exchanges of energy, water and carbon between continents and atmosphere, *Science*, 275, 502–509, doi:10.1126/science.275.5299.502.

Simpson, J., R. F. Adler, and G. R. North (1988), A proposed Tropical Rainfall Measuring Mission (TRMM) satellite, *Bull. Am. Meteorol. Soc.*, 69, 278–295, doi:10.1175/1520-0477(1988)069<0278:APTRMM>2.0.CO;2.

Smagorinsky, J. (1963), General circulation experiments with the primitive equations. Part I: The basic experiment, *Mon. Weather Rev.*, 91, 99–164, doi:10.1175/1520-0493(1963)091<0099:GCEWTP>2.3.CO;2.

Smith, R. C. G., and B. J. Choudhury (1990), On the correlation of indices of vegetation and surface temperature over south-eastern Australia, *Int. J. Remote Sens.*, 11, 2113–2120, doi:10.1080/01431169008955164.

Taylor, C., E. F. Lambin, N. Stephenne, R. Harding, and R. Essery (2002), The influence of land-use change on climate in the Sahel, *J. Clim.*, 15, 3615–3629, doi:10.1175/1520-0442(2002)015<3615:TIOLUC>2.0.CO;2.

Tian, Y., R. E. Dickison, L. Zhou, and M. Shaikh (2004), Impacts of new land boundary conditions from Moderate Resolution Imaging Spectroradiometer (MODIS) data on the climatology of land surface variables, *J. Geophys. Res.*, 109, D20115, doi:10.1029/2003JD004499.

Valor, E., and V. Caselles (1996), Mapping land surface emissivity from NDVI: Application to European, African, and South American areas, *Remote Sens. Environ.*, 57, 167–184, doi:10.1016/0034-4257(96)00039-9.

Walko, R. L., et al. (2000), Coupled atmosphere-biophysics-hydrology models for environmental modeling, *J. Appl. Meteorol.*, 39, 931–944, doi:10.1175/1520-0450(2000)039<0931:CABHMF>2.0.CO;2.

Wan, Z., Y. Zhang, Q. Zhang, and Z.-L. Li (2004), Quality assessment and validation of the MODIS global land surface temperature, *Int. J. Remote Sens.*, 25, 261–274, doi:10.1080/0143116031000116417.

Wang, Y., et al. (2004), Evaluation of the MODIS LAI algorithm at a coniferous forest site in Finland, *Remote Sens. Environ.*, 91, 114–127, doi:10.1016/j.rse.2004.02.007.

Williams, C. N., A. Basist, T. C. Peterson, and N. Grody (2000), Calibration and verification of land surface temperature anomalies derived from the SSM/I, *Bull. Am. Meteorol. Soc.*, 81, 2141–2156, doi:10.1175/1520-0477(2000)081<2141:CAVOLS>2.3.CO;2.

Xue, Y. (1997), Biosphere feedback on regional climate in tropical north Africa, *Q. J. R. Meteorol. Soc.*, 123, 1483–1515, doi:10.1002/qj.49712354203.

Yucel, I. (2006), Effects of implementing MODIS land cover and albedo in MM5 at two contrasting U.S. regions, *J. Hydrometeorol.*, 7, 1043–1060, doi:10.1175/JHM536.1.

Zhou, L., et al. (2003), A sensitivity study of climate and energy balance simulations with use of satellite-derived emissivity data over North Africa and Arabian Peninsula, *J. Geophys. Res.*, 108(D24), 4795, doi:10.1029/2003JD004083.

————————

J. Ge, Department of Geography, Oklahoma State University, 225 Scott Hall, Stillwater, OK 74078-4073, USA. (jianjun.ge@okstate.edu)

B. Lofgren, Great Lakes Environmental Research Laboratory, NOAA, 2205 Commonwealth Boulevard, Ann Arbor, MI 48105-2945, USA.

J. Qi, Department of Geography, Michigan State University, 116 Geography Building, East Lansing, MI 48824-1115, USA.